AIAA JOURNAL
Vol. 62, No. 4, April 2024

Analysis of Geometric and Material Nonlinearity in the Column Bending Test

Ajay Harihara Sharma*
University of Colorado, Boulder, Colorado 80309
Thomas J. Rose† and Nicholas Bearns‡
Redwire, Longmont, Colorado 80503
Thomas W. Murphey§
Opterus Research and Development, Inc., Loveland, Colorado 80537
and
Francisco López Jiménez¶
University of Colorado, Boulder, Colorado 80309

https://doi.org/10.2514/1.J063247

The column bending test (CBT) is an experimental method to measure the moment–curvature behavior and failure curvature of high-strain composites (HSCs), designed to apply a relatively constant bending moment through a sample up to very high curvatures. In this paper, we first calculate the errors involved in the simplified geometric analysis used to model the CBT by considering two different effects: variations in the bending moment through the sample and nonlinearities in the material response of the fibers. The first effect, modeled using Euler's elastica, results in a set of design guidelines for the test geometry (i.e., length of the grips and the specimens) in order to achieve moderate errors in moment and curvature predictions. The nonlinearity in the fiber behavior (tension stiffening and compression softening) does not have a strong effect on the curvature but produces significant variations in the bending stiffness of HSCs as well as the maximum strain observed in the fibers due to the shift in the neutral axis. This indicates that accounting for the nonlinear behavior of fibers is necessary in order to accurately predict the failure properties of HSCs under bending.

Nomenclature

A_{el}	=	value of variable A predicted by the elastica solution
A_g	=	value of variable A predicted by the geometry-based closed-form solution
a	=	horizontal distance between center and ends of the coupon
D_{11}	=	bending stiffness in the fiber direction
D_{110}	=	initial bending stiffness
d_{initial}	=	distance between pins when the specimen is straight
d_{test}	=	distance between pins during the test
E_f	=	nonlinear fiber stiffness, varying as a function of applied strain ε
$E_{f,0}$	=	initial fiber stiffness
E_0	=	initial composite stiffness
L	=	total length of the setup
l	=	effective length of the rigid fixture arm
l_s	=	free length of specimen
M	=	bending moment
M_{max}	=	maximum moment occurring at the center of the bent specimen
M_{min}	=	minimum moment occurring at the coupon edges
N	=	normal axial force
P	=	load applied to the fixture by the testing machine
R	=	radius of curvature of the bent coupon
r	=	effective moment arc length
s	=	arclength along the specimen
t	=	specimen thickness
V_f	=	fiber volume fraction in the composite
x_m	=	boundary condition at the symmetry point
y_{na}	=	position of neutral axis
β	=	angle between vertical axis and tangent vector at every point of bent coupon
γ	=	nonlinear material parameter, determined empirically
Δx	=	horizontal distance between joint and point where specimen leaves rigid arms, for zero applied curvature
Δy	=	vertical distance between joint and point where specimen leaves rigid arms, for zero applied curvature
δ	=	vertical displacement of testing machine
ε	=	nominal strain assuming neutral axis remains at center of the specimen
$\varepsilon_{C,\text{cr}}$	=	critical compressive strain, where instantaneous modulus becomes zero
ζ_κ	=	correction factor for curvature
ζ_D	=	correction factor for bending stiffness
θ	=	initial angle of fixture arm
κ	=	curvature of bent specimen
ξ	=	ratio of total size of rigid arms to specimen freelength
σ_c	=	homogenized stress in the composite laminate
ϕ	=	change in fixture arm angle due to deflection of testing machine

Presented as Paper 2019-1746 at the AIAA SciTech Forum, San Diego, CA, January 7–11, 2019, and as Paper 2021-0196 at the AIAA SciTech Forum, Virtual Event, January 11–15 and 19–21, 2021; received 4 June 2023; revision received 15 November 2023; accepted for publication 17 November 2023; published online 22 December 2023.

*Graduate Student, Ann and H. J. Smead Department of Aerospace Engineering Sciences. Student Member AIAA.

†Senior Analysis Engineer IV; also Graduate Student, Ann and H. J. Smead Department of Aerospace Engineering Sciences, University of Colorado, Boulder, Colorado 80309; currently Principal Engineer, Loft Federal, Inc. Member AIAA.

‡Structural Analyst; also Graduate Student, Ann and H. J. Smead Department of Aerospace Engineering Sciences, University of Colorado, Boulder, Colorado 80309; currently Structural Analyst, Tendeg.

§President, 815 14th Street. Associate Fellow AIAA.

¶Assistant Professor, Ann and H. J. Smead Department of Aerospace Engineering Sciences; francisco.lopezjimenez@colorado.edu. Senior Member AIAA (Corresponding Author).

I. Introduction

SEVERAL designs of deployable space structures are based on the elastic deformation of structural elements during stowage, and the subsequent deployment by releasing the stored strain energy.

Examples include continuous longeron masts [1], antenna booms [2], spring-back reflectors [3], large deployable antennas [4], tape-spring trusses [5], and deployable solar arrays [6]. To further increase their packaging efficiency, these architectures require materials able to achieve large curvatures during stowage. Of particular interest are high-strain composites (HSCs) [7], a class of fiber composite structures designed to operate at strains higher than 1% when subjected to bending. These are often thin unidirectional carbon fiber laminates or FlexLams [8], laminates with $[\pm 45/0/\pm 45]$ orientation to reinforce buckling and loading in the nonzero directions. Despite their promising mechanical properties, the application of HSCs is hindered by the lack of analytical and numerical tools able to reliably and accurately predict their failure curvature [9]. The reason is the combination of complex micromechanics controlling laminate failure [10], size effects on thin laminates [11], and time-dependent behavior after the long stowage periods expected in a space mission [12–14]. To shed light on the unique failure properties of HSCs, several recent studies have focused on the testing of their large curvature bending behavior [9,15–39]. A key goal of this experimental campaign is the development of a reliable and well-characterized testing procedure.

The experimental determination of the high-curvature bending behavior of HSCs, including their failure curvature, requires a test able to subject thin composite laminates to very high curvatures, sometimes in the range $\kappa > 0.4\ \text{mm}^{-1}$ (i.e., radius of curvature in the order of a few millimeters). Traditional bending testing techniques, such as three- and four-point bending, are designed for small deflections in the linear regime. Even if the analysis of the test was expanded to account for large deflections, these setups have difficulty achieving the very small radius of curvature necessary to produce failure in thin composite laminates. Several alternative techniques have been explored. The large-deformation four-point bending test is able to produce the required high curvatures, but the abrupt transition of the stress state at the grips leads to premature failure of the coupons [18]. The platen test has also been used to test the failure curvature of thin composite laminates [16], but the moment distribution throughout the specimen is highly nonuniform, leading to large errors in the processing of results unless the large deformation behavior is modeled correctly. Yu and Hanna developed an apparatus able to apply pure bending on thin sheets, but with limitations on the possible maximum strain achieved [40].

The column bending test (CBT) [20,22–26] is able to overcome these shortcomings, loading the coupons with a nearly constant bending moment that results in failure close to the center of the coupon. The setup can be seen in Fig. 1. It uses pins and ball bearings to turn the vertical displacement of the testing machine into rotation of the grips, resulting in bending of the coupon. If the coupon is sufficiently shorter compared to the length of the arms, the variation of the bending moment within the specimen is small, which results in close to uniform curvature, and makes it possible to analyze the test using simple geometric arguments. The error of this approximation depends on the geometry of the arms and the composite coupon, which in turn depend on the thickness of the specimen and the desired maximum bending strain during the test. As a result, sometimes the variations of curvature within coupons are significant [28,41].

The objective of the present study is to evaluate the validity of the assumptions used to process the results of the CBT test and provide a series of testing recommendations. In particular, we compare the maximum curvature calculated assuming constant curvature through the specimen, with the prediction obtained analyzing the test using Euler's elastica theory, which models the behavior of slender bodies subjected to large deflections. Our results provide the error between both predictions as a function of the ratio between the two main geometry parameters of the test (size of the grips and free length of the tested coupon), and they can be used to determine when a simple geometrical analysis is able to produce an accurate prediction of the maximum curvature in the specimens. Finally, we also explore the effect of material nonlinearity in the laminate by quantifying the shift of neutral axis and its effect on stresses and strains.

The structure of the paper is as follows: Section II provides a background of the CBT. Section III explains the model used to capture possible nonlinearities in the fiber behavior. In Sec. IV, we then explain the elastica theory that is used to predict the variations in curvature across the specimen. Section V discusses the comparison of moment–curvature predictions obtained through the closed-form solution, and the elastica theory for various cases of softening observed in HSCs, and finally Sec. VII discusses the effects of softening on the local stresses and strains in the fiber.

II. Column Bending Test

The main objective of the CBT is to obtain the moment versus curvature behavior in the geometrically nonlinear regime for thin composite laminates. The slope of moment versus curvature curve provides the value of bending stiffness (D_{11}) for a particular choice of layup as a function of the applied curvature, revealing possible material nonlinearities. The test also provides the failure curvature of the material, which is one of the main parameters necessary for the design of deployable space structures using HSCs. The goal of this section is to review the experimental setup, and the closed-form that can be developed assuming constant curvature in the sample.

A. Description of the Experimental Setup

The CBT is designed to characterize the bending behavior of thin coupons at large curvatures in a universal testing machine. The rigid arms holding the specimen are connected through ball bearings to two rotary shafts to reduce friction, which remain horizontal and parallel during the test (see Fig. 1). Each of the shafts is connected to a U-shaped clevis, which are in turn attached to the testing machine. As the cross-head of the testing machine moves down, the shafts move closer together, and the rigid arms rotate. The grip holding the specimen is one side of the rigid arms, next to the joint connection. Since the loads observed in the test are usually small, friction is usually sufficient to prevent the specimen from slipping, but it is important to reduce the

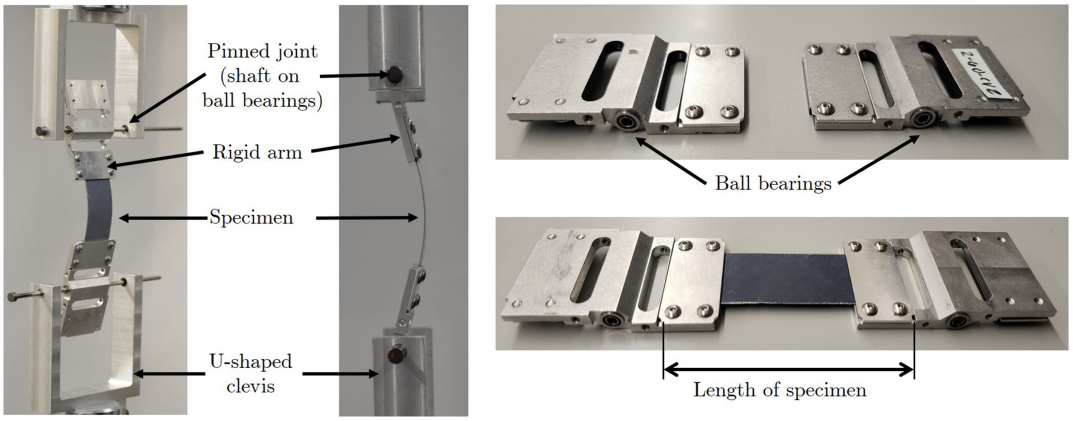

Fig. 1 Image of the experimental setup used in the column bending test.

effect of gravity. Two strategies are commonly used for the same. First, the fixture is sometimes built with polymers through rapid prototyping. Second, the fixture can be designed using arms that are symmetric around their connection to the shaft, so that they are balanced in the absence of loading. Due to symmetry, lack of gravity effects, and the pinned boundary conditions, there is no reaction moment on the grip. In either case, it is important to ensure that the specimen remains flat and that the reaction forces are not able to bend the grips, since that would distort the initial angle of the specimen. The bending moment in the specimen is equal to the vertical force on the grips, which is recorded by the testing machine times the horizontal distance from specimen to the pins. This greatly simplifies the calculation of the bending moment. Curvature is often calculated using the displacement of the cross-head and geometric considerations, although other studies have used noncontact image-based methods to directly track curvature and strain [13,26].

If the specimen is initially straight and aligned with the loading axis, the loading will first compress the coupon until buckling takes place, resulting in bending of the specimen. To reduce this initial buckling and to ensure that the coupon bends in a previously determined direction, two alternatives can be used. First, the test can be started with the coupon already bent, introducing a small initial curvature. Alternatively, the coupons are offset from the loading axis (i.e., the pinned joints where the arms meet the U-shaped clevis) by a small distance, so that a small bending moment is introduced at the beginning of the test. Regardless of the approach followed, as the test progresses, the distance between sample and loading axis increases rapidly, and the axial and shear loading in the coupon can be neglected compared to the bending moment.

B. Geometric Analysis

During the CBT, the bending moment along the coupon varies linearly with the distance to the loading axis, with the minimum at the grip and the maximum and the center of the specimen. If the relative difference between both distances is small and the material properties are linear, it is possible to assume that the bending moment and therefore the curvature are close to constant along the arc length. It is also assumed that the length of the specimen remains constant during the test, since the compressive loading is negligible compared to the bending moment. This greatly simplifies the analysis, and it is possible to provide a closed-form estimation of the maximum curvature and bending moment. The main objective of this paper is to explore the regime where this assumption yields accurate results. The geometric closed-form solution has already been previously discussed [23,26,28], but it will be also presented here for completion.

In Fig. 2, l_s represents the free length of the samples between the rigid arms or gauge length (assumed to be constant during the test), l represents the effective length of the rigid fixture arm (i.e., the distance between sample and pin), θ represents the initial angle of the fixture arm, and ϕ represents the change in fixture arm angle due to deflection during the test. The testing machine provides a vertical displacement δ and records the load applied to the fixture, P. The effective moment arc length is denoted by r, a represents the horizontal component of the distance between center and end of the coupon, and R represents the radius of curvature of the bent coupon, which is assumed to be constant.

From Fig. 2a, we can see that the position of the pinned joint and the position from where the specimen leaves the rigid arm are offset. This distance is given by Δx. As mentioned above, this offset parameter helps ensure that the specimen always bends in the desired direction as the test proceeds. We assume that the specimen leaves the rigid arm at a perfect 90° angle. As a result of this assumption, the sum of the angles by which the two rigid arms rotate (ϕ) is equal to the angle subtended by the arc at the center of the assumed circle. This greatly simplifies the calculations, since curvature can now be obtained using the radius of curvature (R), freelength (l_s), and the central angle (ϕ).

To evaluate the central angle (ϕ), we can make use of the fact that the change in distance between the pin joints is equal to δ (see Fig. 2). At the beginning of the test, the distance between the grips is equal to

$$d_{\text{initial}} = 2l\cos\theta + l_s \tag{1}$$

Once the test starts and each of the arms undergoes an angular rotation of $\phi/2$ as a result of the vertical displacement δ, the vertical distance between the shafts is given by

$$d_{\text{test}} = 2R\sin(\phi/2) + 2l\cos(\theta + \phi/2) \tag{2}$$

Upon applying $d_{\text{initial}} = d_{\text{test}} + \delta$, we obtained an equation for ϕ, as a function of the geometry of the test and the applied displacement δ:

$$\frac{\delta}{l_s} = 1 - \frac{2}{\phi}\sin\frac{\phi}{2} + 2\frac{l}{l_s}\left(\cos\theta - \cos\left(\theta + \frac{\phi}{2}\right)\right) \tag{3}$$

The above equation is transcendental and requires a numerical solution. As mentioned above, the curvature can now be obtained using the definition of curvature, $\kappa = 1/R$, and the formula for arclength of a circle, $l_s = R\phi$, yielding

$$\kappa = \frac{\phi}{l_s} \tag{4}$$

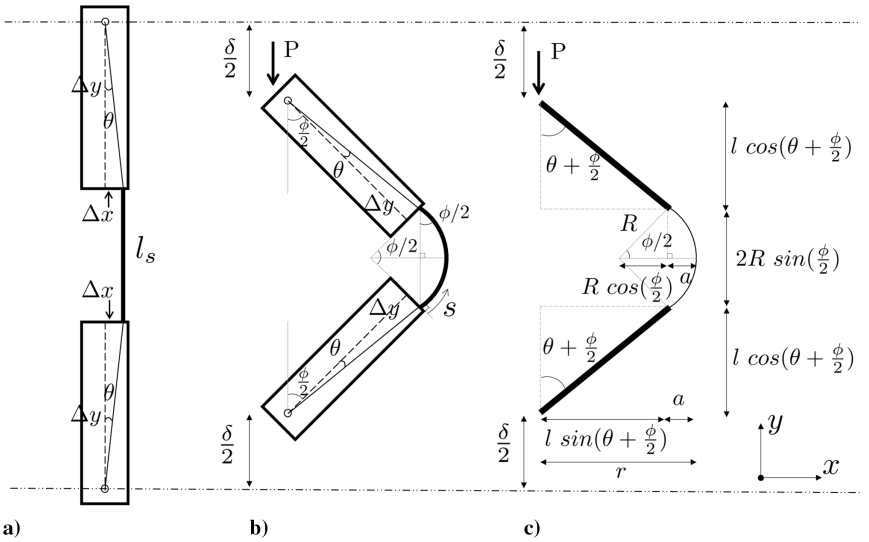

Fig. 2 Geometry of the column bending test: a) initial test geometry, b) angles, and c) distances in the test setup when a displacement δ is applied.

Assuming that the neutral axis always remains at the center of the specimen during bending, the strain can be calculated using the curvature κ and thickness t and is given by

$$\varepsilon = \frac{\kappa t}{2} = \frac{\phi t}{2l_s} \tag{5}$$

To compute the maximum moment $M_{\max}$, we first calculate the effective moment arm length r. As seen from Fig. 2c, the distance r is given by

$$r = a + l\sin\left(\theta + \frac{\phi}{2}\right) \tag{6}$$

From Fig. 2c, we can also see that

$$a = R - R\cos\left(\frac{\phi}{2}\right) \tag{7}$$

Substituting the expression of a in the expression for r and dividing it by s, we obtain

$$\frac{r}{s} = \frac{1}{\phi}\left(1 - \cos\frac{\phi}{2}\right) + \frac{l}{s}\sin\left(\theta + \frac{\phi}{2}\right) \tag{8}$$

The maximum moment occurs at the center of the specimen and is given by

$$M_{\max} = Pr \tag{9}$$

The minimum moment occurs at the coupon edges near the grips. It is given by

$$M_{\min} = Pl\sin\left(\theta + \frac{\phi}{2}\right) \tag{10}$$

Next, we consider two ways in which the reality could deviate from this simplified geometric analysis. First, the effect of material nonlinearities is discussed. After that, the effect of nonconstant bending moment along the arc-length of the specimen is discussed by utilizing the theory of elastica.

III. Stiffness Nonlinearity in High-Strain Composites

The nano-structure of carbon fiber consists of sheets of carbon atoms, which are not completely aligned with the fiber direction. As a result, carbon fibers are inherently nonlinear [42]: they stiffen under tension, as the sheets rotate to align with the fiber direction, and soften under compression. The same behavior can be observed in carbon fiber laminates loaded under tension [43] or bending [30,36]. Several constitutive relationships have been proposed to determine and model this nonlinear behavior [43–47]. Here we use the empirical approach proposed by Van Dreumel and Kamp [48], which found that adding a quadratic dependence to the stress–strain relationship resulted in a very good approximation for most carbon fibers. Assuming that the nonlinearity is the same in tension and compression, the modulus of the fibers, E_f, is given by

$$E_f(\varepsilon) = E_{f,0}(1 + \gamma\varepsilon) \tag{11}$$

where $E_{f,0}$ is the initial stiffness of the fiber, ε is the applied strain, and γ is a parameter that determines the level of nonlinearity. In our case, for tensile stiffnening, we have that $\gamma > 0$.

In addition to the nonlinearity inherent to the response of the fibers, there are other possible reasons for a laminate to exhibit nonlinear behavior. These include possible plastic and viscous behavior of the matrix, geometric nonlinearity due to initial fiber waviness, as well as rearrangement of the microstructure due to complex the fiber architecture, particularly in woven laminates. However, previous research has shown that, assuming the same quadratic behavior in Eq. (11) for the mechanical response of the laminate, and not just the fibers, can be used to accurately characterize the bending behavior of thin laminates [17,19]. We follow the same approach and assume that the stress–strain relationship in the direction of bending is given by

$$\sigma_c = E_0\varepsilon + \frac{E_0\gamma\varepsilon^2}{2} \tag{12}$$

where σ_c is the stress in the laminate, considered as an average (i.e., homogenized) value, E_0 is the initial longitudinal modulus of the laminate, and γ is again a parameter describing the nonlinearity of the mechanical response. This constitutive relationship is shown in Fig. 3 for different values of γ.

As expected, the resulting stress–strain relationship shows stiffening during tension and softening during compression, which in the case of bending results in a shift of the neutral axis to the tensile side. Furthermore, according to this constitutive model, there also exists a critical compressive strain ($\varepsilon_{C,\mathrm{cr}} = -1/\gamma$) where the instantaneous modulus becomes zero (marked with a star symbol in Fig. 3). Beyond this point, the modulus becomes negative, until eventually tension is observed on the compression side (see Fig. 3). This is a limitation of our simple empirical model, which is not able to capture the complicated compressive behavior of carbon fibers, which after a softening region exhibits a plateau of constant stress that can reach extremely large deformations [47,49]. To avoid presenting nonphysical results, the analysis presented in Secs. V and VII will indicate the point in which $\varepsilon_{C,\mathrm{cr}}$ is reached at any point in the laminate.

Utilizing the above assumptions, we can develop a simplified expression for the moment–curvature relationship, the bending stiffness in the fiber direction (D_{11}), and the expression that quantifies the shift in neutral axis. To do so, we first utilize the equilibrium of internal forces through the thickness to determine the position of the neutral axis. This is given by

$$N = \int_{-t/2}^{t/2} \sigma_c \mathrm{d}y = 0 \tag{13}$$

Here, the laminate stress σ_c is a function of the strain ε given by the constitutive relationship, Eq. (12). We need to determine the strain as a function of the thickness coordinate in order to establish the equilibrium of the forces through the thickness. Using Euler–Bernoulli theory, we obtain the relation

$$\varepsilon = \kappa(y - y_{\mathrm{na}}) \tag{14}$$

where κ is the curvature and y_{na} is the position of the neutral axis. Solving Eqs. (12–14) gives the expression for the neutral axis. This is given by

$$y_{\mathrm{na}} = \frac{6 - \sqrt{36 - 3t^2\gamma^2\kappa^2}}{6\gamma\kappa} \tag{15}$$

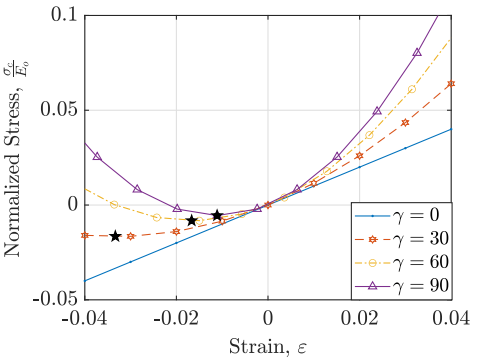

Fig. 3 Normalized stress vs strain for four different values of the parameter γ describing fiber nonlinearity.

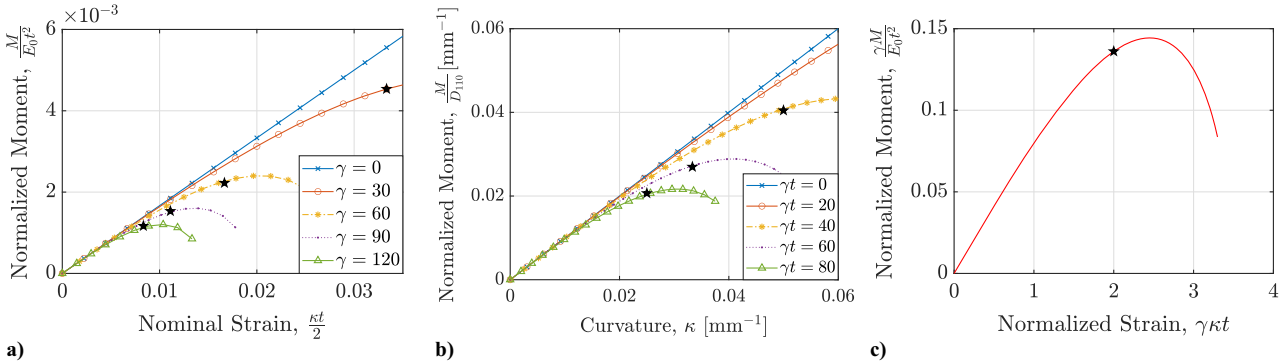

Fig. 4 Plots for normalized moment as a function of a) nominal strain ($kt/2$), b) curvature (κ), and c) nominal strain scaled by 2γ ($\gamma\kappa t$).

The bending moment per unit width can be evaluated using the following relation:

$$M = \int_{-t/2}^{t/2} \sigma_c (y - y_{\text{na}})\, \mathrm{d}y = 0 \tag{16}$$

Utilizing the expression for stress from Eq. (12), strain from Eq. (14), and neutral axis from Eq. (15), we obtain the following expression for the bending moment:

$$M = \frac{1}{72} E_0 \kappa t^3 \sqrt{36 - 3t^2\gamma^2\kappa^2} \tag{17}$$

The bending stiffness D_{11} is given by

$$D_{11} = \frac{\partial M}{\partial \kappa} = \frac{E_0 t^3 (6 - t^2\gamma^2\kappa^2)}{12\sqrt{36 - 3t^2\gamma^2\kappa^2}} \tag{18}$$

Having established the moment versus curvature relationship in Eq. (17), we observe the trend resulting from three different possible normalizations. Figure 4 plots the expression for normalized moment as a function of nominal strain ($\kappa t/2$), curvature (κ), and nominal strain scaled by 2γ ($\gamma\kappa t$), respectively. Despite the non-standard normalization of the bending moment, the results in Fig. 4a are useful because the softening is governed simply by γ,with no thickness dependence, and so it illustrates the nominal strain at which the behavior deviates from linear for different levels of material softening. We can also see that as γ increases, the critical strain ($\varepsilon_{C,\text{cr}}$) is obtained at a lower nominal strain value. Figure 4b shows the bending moment normalized by the initial bending stiffness, $D_{110} = E_0 t^3/12$, as a function of curvature. In this case, the softening is controlled by the parameters γt, and so it can be used as a direct design guideline for picking a given combination of laminate thickness and type of fibers (i.e., a given value of γ). The normalization in Fig. 4c incorporates the softening into the normalized strain ($\gamma\kappa t$), allowing for all previous results to collapse into a single master curve.

IV. Analysis Using Elastica Theory

The closed-form solution based on the geometric analysis presented in Sec. II.B assumes a small variation of bending moment across the arclength of the specimen, so that the curvature can be assumed to be constant. If this is not true, the behavior of the coupon needs to be modeled using Euler's theory of elastica, which accounts for large-scale deflection of slender structural elements. We use the same geometry presented in Fig. 2, and for our analysis, Δx is considered to be zero, since it has been shown that it plays a relatively minor role in the moment–curvature response [35]. This not only simplifies the analysis but leaves only two independent length parameters, the length of the arms, l, and the free length of the sample, l_s, so that the solution is self-similar.

Assuming that the specimen is inextensible, we utilize the constitutive equation

$$\begin{aligned} M(s) &= \frac{1}{72} E_0 t^3 \kappa(s) \sqrt{36 - 3t^2\gamma^2\kappa(s)^2} \\ &= \frac{1}{72} E_0 t^3 \beta'(s) \sqrt{36 - 3t^2\gamma^2\beta'(s)^2} \end{aligned} \tag{19}$$

where $M(s)$ represents the bending moment per unit width at every point along the arclength s, E_0 represents the initial Young's modulus, $\kappa(s)$ is the curvature along the arclength, and β represents the angle between the vector tangent to the coupon and the vertical axis at every point along the curve. In the case of no-softening, $\gamma = 0$, we recover the familiar expression

$$M(s) = D_{110}\kappa(s) = \frac{E_0 t^3}{12}\beta'(s) = \frac{E_0 t^3}{12}\frac{d\beta}{ds} \tag{20}$$

The differential equations for the position coordinates $x(s)$ and $y(s)$ can be given in terms of the angle $\beta(s)$ as

$$\frac{dx}{ds} = \sin\beta \tag{21}$$

$$\frac{dy}{ds} = \cos\beta \tag{22}$$

For the geometry of the problem, equilibrium of bending moment yields

$$\frac{1}{72} E_0 t^3 \frac{d\beta}{ds} \sqrt{36 - 3t^2\gamma^2\left(\frac{d\beta}{ds}\right)^2} = M = P\left(x + l\sin\frac{\phi}{2}\right) \tag{23}$$

The above equation can be integrated numerically in MATLAB using the "ode45" command. The boundary conditions are $x(0) = 0$ and $y(0) = 0$ at the initial point and $\theta(l_s/2) = 0$ and $x(l_s/2) = x_m$ at the symmetry point, where x_m represents the imposed x-coordinates of the midpoint of the specimen, used to describe the evolution of the test. Since not of all of the conditions can be expressed as initial boundary conditions, a shooting algorithm has been implemented, which calculates the applied loading, as well as the angle rotated by the rigid arms ($\phi/2$) necessary to satisfy the conditions $\theta_{\text{midpoint}} = 0$ and $x_{\text{midpoint}} = x_m$. The numerical integration provides the shape of the specimen for each applied vertical displacement δ, as well as the distribution of curvature across the arclength, $\kappa(s)$.

V. Comparison of Moment–Curvature Predictions

We now compare the prediction for the bending moment, curvature, and bending stiffness provided by the closed-form equation obtained through the simplified geometric analysis, and the numerical integration of the elastica, for varying degrees of softening of the bent specimen. A preliminary analysis, not using the theory of elastica, was presented previously in [24]. For this study, the thickness of the specimen is normalized by l_s, and a range of $t/l_s = \{0.005, 0.03\}$ has been used, based on typical values reported in

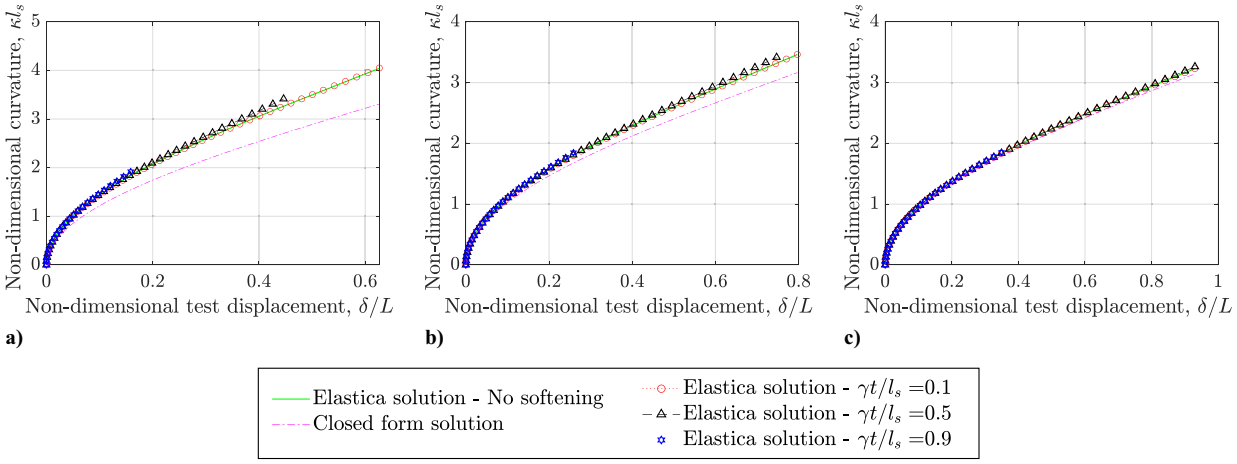

Fig. 5 Curvature as a function of the applied vertical displacement, δ/L, predicted by the geometric solution and the integration of the elastica, for a) $\xi = 0.5$, b) $\xi = 2$, and c) $\xi = 8$.

literature as used to test HSC to failure under bending. The values for γ were chosen to vary between 20 and 30, representative of values reported in the literature [21]. Thus, three values for $\gamma t/l_s$ were obtained using the above parameters (0.1, 0.5, and 0.9) and are used to represent different ranges of softening. Moreover, for all the cases, it is assumed that $\Delta x = 0$, so the only geometric parameters that appear in the problem are l and l_s. We define the total arclength of the setup from joint to joint, including the grips, as

$$L = 2l + l_s \tag{24}$$

Several normalizations have been incorporated here in order to make our results general. First, the curvature has been normalized by l_s. The normalized variable κl_s represents the approximate angle subtended by the bent specimen (in fact, it would be equal to be subtended angle if the curvature was constant). The moment has been normalized in two ways—first, by the initial bending stiffness D_{110}. This helps obtain a linearized version of the curvature, and the value would be exactly equal to the curvature if the material was linearly elastic. The second normalization for the moment is given by Ml_s/D_{110}. In the case of a linearly elastic material, it is equal to the normalization of the curvature, κl_s. This particular normalization helps obtain a nondimensional moment so that our results incorporate all possible cases of the initial bending stiffness and the coupon free length. The nonlinear bending stiffness D_{11} has been normalized by the linear bending stiffness (which is also the initial bending stiffness), D_{110}. The test displacement has been normalized by L, so that the quantity δ/L represents the relative test displacement with respect to the total arclength L such that the test displacement value does not depend on the coupon free length or the size of the rigid arms. The theoretical range for δ/L is [0,1], with $\delta/L = 0$ corresponding to the two pins overlapping. The arclength along the specimen, s, has been normalized by l_s, so that it varies in the [0, 1] interval.

The geometry of the test can then be defined by a single parameter, the normalized free length ξ, defined as

$$\xi = \frac{2l}{l_s} \tag{25}$$

which describes the ratio of the combined length of the rigid arms, $2l$, with respect to the specimen freelength, l_s. Larger values of ξ correspond to rigid arms that are relatively longer compared to the specimen freelength.

The maximum curvature predicted by elastica as well as the geometric analysis for different values of ξ is presented in Fig. 5, as a function of the normalized vertical displacement during the test, δ/L. The results clearly show that the prediction provided by the closed-form solution based on geometric considerations is more accurate for large values of ξ, which correspond to cases in which the length of the arms is large compared to the coupons. It can also be seen that softening plays a greater role for small values of ξ, where the deviations between the various elastica solutions and the closed-form solution are much higher, compared to cases involving larger values of ξ, where the differences between various cases of softening and the nonsoftening elastica solution, as well as the closed-form solution, are negligible.

The curvatures presented in Fig. 5 represent the maximum curvature along the arclength of the sample, which due to symmetry takes place in the middle point, where the bending moment is maximum. Figure 6 presents the nondimensional curvature as a function of the arclength of the sample, for the same three values of ξ and applied

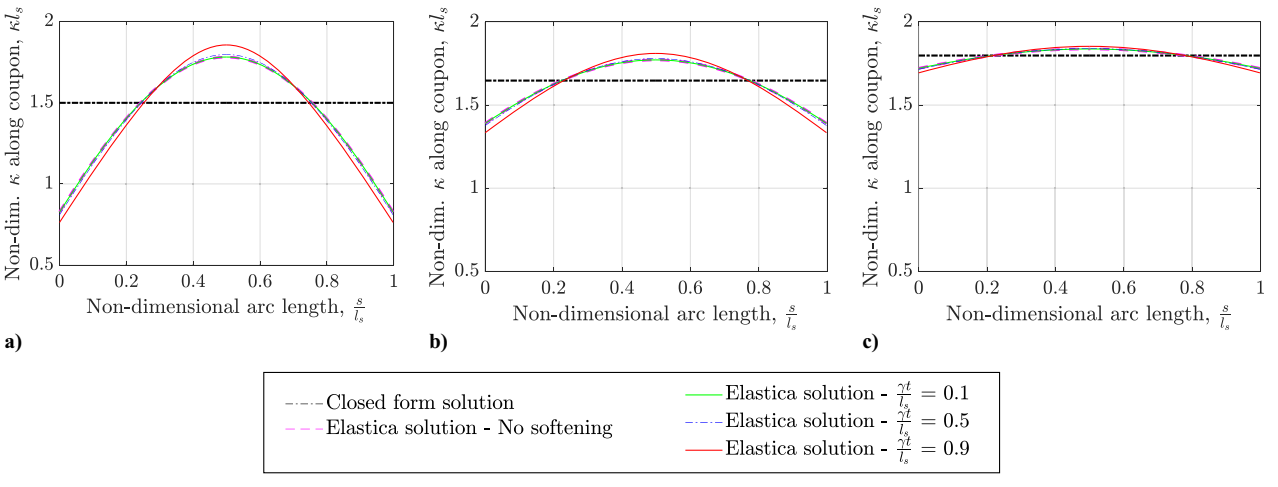

Fig. 6 Variation of the curvature along the arclength for a) $\xi = 0.5$, $\delta/L = 0.15$; b) $\xi = 2$, $\delta/L = 0.25$; and c) $\xi = 8$, $\delta/L = 0.35$.

vertical displacements of $\delta/L = 0.15$, $\delta/L = 0.25$, and $\delta/L = 0.35$ for $\xi = 0.5$, $\xi = 2$, and $\xi = 8$, respectively. These values of δ/L were chosen for being very close to the test displacement value resulting in zero stiffness in the compression side of the laminate, for the case with the highest softening considered, $\gamma t/l_s = 0.9$.

Figures 7a–7c show the maximum moment predicted by the elastica, and the closed-form solution, as a function of the maximum curvature on the specimen (obtained at the center of the specimen). The points on the line $y = x$ represent a linear relation between the normalized moment M/D_{110} and the curvature κ. For different values of softening, the elastica curves deviate from this straight line due to material nonlinearity. In the case of the closed-form solution, deviations are a combination of material softening and errors due to the assumption of the constant curvature. We can see that the errors in the closed-form solution (i.e., the relative difference between the closed-form solution and its corresponding elastica solution) reduce as ξ is increased. As mentioned earlier, the differences are induced mainly due to error in curvature prediction (and not the moment). This has further implications in the calculation of the bending stiffness of the specimen. From the plots, we can observe the difference in the slopes of the two solutions, which is indicative of the error in the bending stiffness predicted by the closed-form solution. For higher values of ξ, the slopes converge, indicating a relatively smaller error in bending stiffness.

Figures 7d–7f show the normalized bending stiffness at the center of the specimen, predicted by the elastica and the closed-form solution, as a function of the normalized vertical displacement during the test, δ/L. The calculation of the moment requires the force as an external input. We assume that the force obtained from the elastica predictions is the true value, and we use that for both the elastica and closed-form solutions calculations of the moment, for a given value of the softening. This is the same process that would be followed when processing experiments, where both the force and displacement can be directly obtained from the testing machine. The bending stiffness given by $\partial M/\partial\kappa$ is then evaluated numerically for each moment–curvature combination.

Figures 7g–7i show the maximum moment predicted by the elastica and the closed-form solution for the same values of ξ as before, as a function of the normalized vertical displacement during the test, δ/L. The results show a relatively small difference between the two predictions, indicating that the errors in bending stiffness ($\partial M/\partial\kappa$) occur mainly due to curvature and not the moment. Also, softening plays a

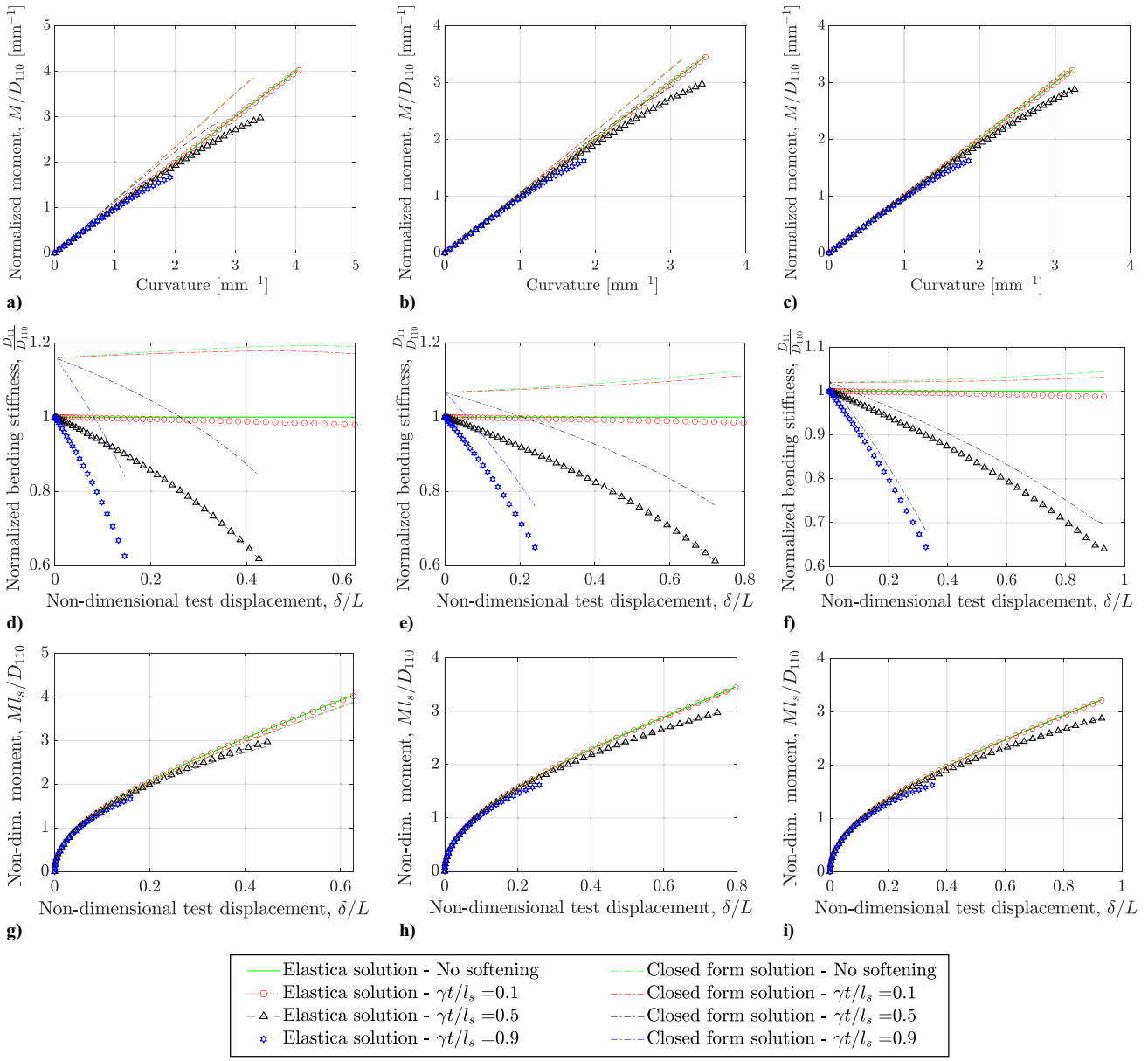

Fig. 7 Normalized moment, bending stiffness, and nondimensional moment as a function of curvature and applied vertical displacement. respectively, predicted by the geometric solution and the integration of the elastica for $\xi = 0.5$ (left), $\xi = 2$ (center), and $\xi = 8$ (right).

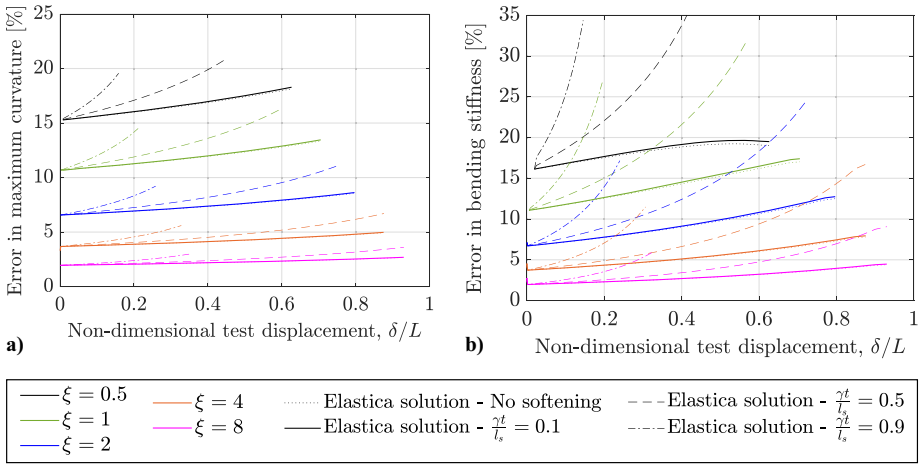

Fig. 8 Error in the prediction of maximum curvature and bending stiffness by the closed-form geometric solution, as a function of the applied vertical displacement, δ/L, and $\xi = 2l/l_s$.

more important role for smaller values of ξ, where its effects are relatively amplified compared to the larger values, similar to curvature.

Figure 8a shows the error in the prediction of maximum curvature value, defined as $(\kappa_{\max,\text{el}} - \kappa_{\max,g})/\kappa_{\max,\text{el}}$, where $\kappa_{\max,\text{el}}$ and $\kappa_{\max,g}$ are the maximum curvature predicted by the elastica and the closed-form geometric solution, respectively. Figure 8b shows a similar error plot for the bending stiffness at the center of the specimen. They have been evaluated in the same way as described previously in the explanation pertaining to Fig. 7. For a given test displacement, the error in bending stiffness at the center of the specimen is given by $(D_{11,\text{el}} - D_{11,g})/D_{11,\text{el}}$, where $D_{11,\text{el}}$ and $D_{11,g}$ are the bending stiffness predicted by the elastica and the closed-form geometric solution, respectively, both calculated at the center of the specimen.

For all values of ξ, the errors slightly increase with the applied displacement, with the effect being more pronounced for smaller values of ξ. For curvature, the error is bounded by 5% for $\xi \geq 8$ and by 12% for $\xi \geq 2$, but it can be significant for low values of ξ. For bending stiffness, the error is bounded by 10% for $\xi \geq 8$ and by 25% for $\xi \geq 2$. All the curvatures and the bending stiffnesses have been computed until the value where the fiber modulus becomes zero, and this value is quite low for cases involving high softening, i.e., for high values of γt. This imposes a restriction on the δ/L value up to which the elastica solution for softening can be computed, thereby explaining the lower δ/L value for the same ξ in Fig. 8. Another observation that results from the plot is that, for smaller values of ξ, softening plays a greater role in the errors involved compared to larger values of ξ. Figure 8 can therefore be used to determine if a given combination of grips and coupon length can be accurately modeled using the simplified geometric analysis, or if it is necessary to consider curvature and the bending stiffness variations.

VI. Correction Factor to Improve the Accuracy of Moment–Curvature Predictions

The previous section characterized the errors that result from the constant curvature assumption used for the closed-form solution that models the CBT. This section provides a correction factor to account for errors incurred when assuming constant curvature. The correction factors will be defined as the ratio between the geometrically exact results obtained through the elastica and those assuming a circle:

$$\zeta_\kappa\left(\xi, \frac{\delta}{L}\right) = \frac{\kappa_{\max,\text{el}}}{\kappa_{\max,g}} \tag{26}$$

$$\zeta_D\left(\xi, \frac{\delta}{L}\right) = \frac{(\partial M/\partial\kappa)_{\text{el}}}{(\partial M/\partial\kappa)_g} \tag{27}$$

where ζ_κ and ζ_D represent the correction factors for curvature and the bending stiffness, respectively, and $\kappa_{\max,\text{el}}$ and $\kappa_{\max,g}$ are the maximum curvatures predicted by the elastica and the closed-form geometric solution, respectively. Additionally, $(\partial M/\partial\kappa)_{\text{el}}$ and $(\partial M/\partial\kappa)_g$ represent the bending stiffness predicted by the elastica and the geometric closed-form solution, respectively. The correction factors ζ_κ and ζ_D are dependent on the parameters ξ and δ/L. This is due to the fact that these correction factors are derived from the errors in curvature and bending stiffness, which are themselves functions of ξ and δ/L.

To obtain a closed-form approximation to the correction factors that does not require solving the nonlinear system of equations governing the Elastica, a fitting was done individually for each of these functions. CBT testing reported in literature typically involves ξ values between 1 and 4. To obtain an accurate fit, 500 equally spaced ξ values were chosen between 0.5 and 8, and correction factors were obtained for each of these using Eqs. (26) and (27) for the case involving no softening.

A parabolic fit was used to capture the variation of the correction factor as a function of $\frac{\delta}{L}$ for each value of ξ. The coefficients of these parabolas were recorded, so as to identify the function that accurately captures the values of these coefficients as a function of ξ. An analytical function for each of the correction factors was then obtained. The MATLAB curve fitting tool was used for this purpose. The correction factor function for curvature can be given by

$$\zeta_\kappa\left(\xi, \frac{\delta}{L}\right) = a(\xi)\left(\frac{\delta}{L}\right)^2 + b(\xi)\left(\frac{\delta}{L}\right) + c(\xi) \tag{28}$$

with parameters

$$a(\xi) = 0.04\xi^{-0.45} - 0.01 \tag{29}$$

$$b(\xi) = 0.03\xi^{-0.6} - 0.005 \tag{30}$$

$$c(\xi) = 0.13\xi^{-0.6} + 1 \tag{31}$$

The correction factor function for bending stiffness can be given by

$$\zeta_D\left(\xi, \frac{\delta}{L}\right) = a(\xi)\left(\frac{\delta}{L}\right)^2 + b(\xi)\left(\frac{\delta}{L}\right) + c(\xi) \tag{32}$$

with parameters

$$a(\xi) = \frac{0.15\xi - 0.125}{\xi^2 - 0.35\xi + 0.3} \tag{33}$$

$$b(\xi) = 0.1\xi^{-0.8} - 0.01 \tag{34}$$

$$c(\xi) = 0.13\xi^{-0.6} + 1 \tag{35}$$

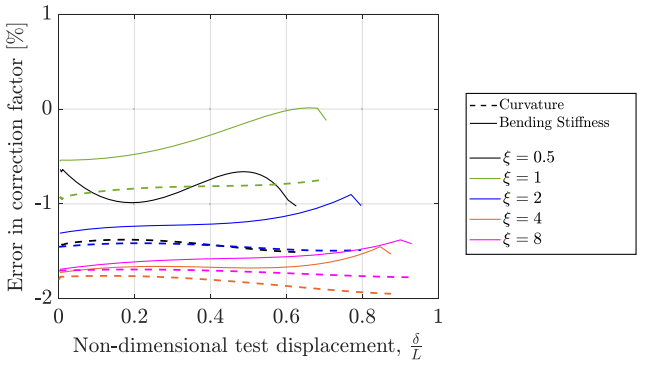

Fig. 9 Comparing the error in correction factor values for both curvature and bending stiffness w.r.t. the elastica solution.

The error between the closed-form expressions in Eqs. (28) and (32) and the exact values for the correction factor is shown in Fig. 9. The errors between the analytical equations and the computed values are within 2%, thereby indicating the validity of the closed-form approximation to the correction factors for the desired range of ξ values between 0.5 and 8. For comparison, the errors are around 20% without the correction factor for $\xi = 0.5$, as observed from Fig. 8.

VII. Effect of Softening on the Local Stresses and Strains in the Fibers

In the previous section, the main emphasis was to explore the effect of variation of the ratio of rigid arms to the specimen freelength, ξ, and the role it plays in the errors involving computation of curvatures for a thin laminate subjected to flexure, as well as to address the errors associated with it. Here, we look at curvature as a way to obtain strain. When there is softening, there is a shift in the neutral axis, such that the maximum strain is no longer $\kappa t/2$. This could have a significant effect even if the change of curvature is not so pronounced. In this section, we calculate the maximum strains as well as the stresses in the compressive and tensile side, for softening.

It should be noted that all the plots have been plotted against nominal strain ($\kappa t/2$). Doing so eliminates any dependency on thickness, so that all the results hold true regardless of the thickness of the specimen, and the only parameter that varies is γ. Since γ is an empirical parameter whose precise value requires complex testing methodologies, it is essential to understand its role in the softening of a thin laminate subjected to flexure. Previous studies [21] have shown that γ typically varies between 20 and 30 for unidirectional laminates with intermediate modulus carbon fibers.

Figure 10a shows the shift in neutral axis that occurs as a result of varying γ. For a nominal strain of 2%, which is representative of the value at which thin specimens fail, the shift in neutral axis is seen to be 6.7, 8.5, and 10.32%, with respect to half the thickness, for γ values of 20, 25, and 30, respectively. This shift in neutral axis is responsible for the variations in stresses and strains on the tension and compression side.

Figure 10b shows the variation in real strain as a function of nominal strain, $\kappa t/2$. The displacement of the neutral surface toward the tension side due to the material nonlinearity results in increased strains in the compression side and reduced strains in the tensile side of the specimen. For a nominal strain of 2%, the compression side experiences strains of 2.135, 2.17, and 2.206% for γ values of 20, 25, and 30, respectively, whereas the tension side experiences strains of 1.865, 1.83, and 1.794%, respectively, for the same values of γ.

Figure 10c shows the variation of maximum stresses as a function of nominal strain, $\kappa t/2$, where both stresses are plotted as absolute values. Here, the shift in the neutral axis is compounded with the material nonlinearity, $\gamma\epsilon^2/2$, and so the difference between tensile and compressive stresses is more pronounced than the difference in strains. As an example, an error of 2.85% is observed in the normalized stress, for γ values of 20 and 30, at a nominal strain of 2% for tension. In contrast, an error of 13.75% is observed for the normalized stress in compression, for the same γ values of 20 and 30, at a nominal strain of 2%. Thus, we can infer that variation of γ plays a relatively minor role for evaluation of tensile stresses, whereas it plays a significant role for the evaluation of compressive stresses.

It is important to remember that both σ_c and ϵ are calculated as stress and strain in the curvature direction, and they are defined in an average sense, without differentiating between fiber and matrix or taking into account stress concentrations in the fibers due to failure of nearby fibers [10,50] or in the matrix due to complex geometry [51,52].

VIII. Conclusions

We have analyzed the CBT, which is used for evaluating the bending behavior of thin composite flexures under large curvature, focusing on the effect of two possible sources of nonlinearity: variations in the bending moment along the sample, and nonlinear material behavior (softening in bending) of the laminate. Both phenomena are described through two nondimensional parameters, so that results are applicable to a wide range of conditions. The geometry of the test is described through ξ, which measures the ratio between the total size of the rigid arms and the specimen freelength, while the material nonlinearity is described by γ, the coefficient for a quadratic term in the stress–strain relationship of the laminate. Both parameters are used to model the test through a nonlinear elastica formulation, which is then compared with a simple geometric analysis that assumes constant curvature along the specimen arclength.

Our results provide guidelines to choose test dimensions that minimize the effects of geometric nonlinearities. We also calculate the expected error in the simplified formulation, as compared to the elastica solution, as a function of the value of ξ and γ. Overall, the simplified geometric analysis of the CBT provides fairly accurate results for large grip sizes, particularly when the combined length of both grips is at least twice the coupon freelength, where the error is around 11%. Two correction factors are provided, so that the results of tests with large nonlinearity can be analyzed without the need of solving the elastica formulation. They have been obtained through fitting to the elastica results and are valid for a wide range of values of ξ and γ, which have been chosen based on the literature.

The present analysis also shows that the effect of the material nonlinearity at the microscale (e.g., changes in maximum stress) can be significantly larger than its effect on macroscopic properties (e.g., moment–curvature relationship). This suggests that a precise

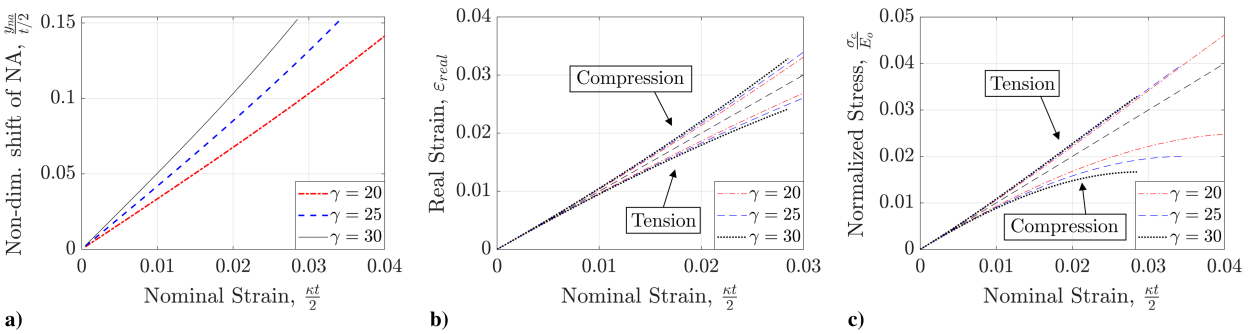

Fig. 10 Comparison of a) shift in neutral axis, b) real strains, and c) real stresses, as a function of varying γ.

description of the mechanical response of the fibers might be necessary when predicting the failure of high-strain composites through modeling at the micromechanic scale, even in cases when it is not necessary to predict the bending stiffness of the laminate. This includes testing of individual fibers to account for their behavior beyond the initial stiffness, but also characterizing matrix properties and fiber architecture as additional sources of nonlinearity in the mechanical response of the laminate.

Acknowledgment

Funding from Redwire Space (formerly Roccor, at the time of the research), through the Air Force Research Lab Small Business Technology Transfer (STTR) Program, contracts FA9453-17-P-0463 and FA9453-19-C-0597, is gratefully acknowledged.

References

[1] McEachen, M., "Validation of SAILMAST Technology and Modeling by Ground Testing of a Full-Scale Flight Article," *48th AIAA Aerospace Sciences Meeting Including the New Horizons Forum and Aerospace Exposition*, AIAA Paper 2010-1491, 2010. https://doi.org/10.2514/6.2010-1491

[2] Mobrem, M., and Adams, D., "Lenticular Jointed Antenna Deployment Anomaly and Resolution Onboard the Mars Express Spacecraft," *Journal of Spacecraft and Rockets*, Vol. 46, No. 2, 2009, pp. 403–410. https://doi.org/10.2514/1.36891

[3] Baier, H., Datashvili, L., Nathrath, N., and Pellegrino, S., "Technical Assessment of High Accuracy Large Space Borne Reflector Antenna," Final Rept. ESA Contract No. 16757/02, 2004.

[4] Soykasap, O., Pellegrino, S., Howard, P., and Notter, M., "Folding Large Antenna Tape Spring," *Journal of Spacecraft and Rockets*, Vol. 45, No. 3, 2008, pp. 560–567. https://doi.org/10.2514/1.28421

[5] Pollard, E., and Murphey, T., "Development of Deployable Elastic Composite Shape Memory Alloy Reinforced (DECSMAR) Structures," *47th AIAA/ASME/ASCE/AHS/ASC Structures, Structural Dynamics, and Materials Conference 14th AIAA/ASME/AHS Adaptive Structures Conference 7th*, AIAA Paper 2006-1681, 2006. https://doi.org/10.2514/6.2006-1681

[6] Spence, B. R., and White, S. F., "Directionally Controlled Elastically Deployable Roll-Out Solar Array," U.S. Patent 8,683,755, file 1 April 2014.

[7] Murphey, T. W., Francis, W., Davis, B., and Mejia-Ariza, J. M., "High Strain Composites," *2nd AIAA Spacecraft Structures Conference*, AIAA Paper 2015-0942, 2015. https://doi.org/10.2514/6.2015-0942

[8] Peterson, M. E., and Murphey, T. W., "Large Deformation Bending of Thin Composite Tape Spring Laminates," *54th AIAA/ASME/ASCE/AHS/ASC Structures, Structural Dynamics, and Materials Conference*, AIAA Paper 2013-1667, 2013. https://doi.org/10.2514/6.2013-1667

[9] Sharma, A. H., Hill, S. A., Perez, R., Rose, T., and Lopez Jimenez, F., "Tensile Fiber Failure on High Strain Composites," *AIAA Scitech 2020 Forum*, AIAA Paper 2020-0208, 2020. https://doi.org/10.2514/6.2020-0208

[10] Breite, C., Melnikov, A., Turon, A., de Morais, A. B., Le Bourlot, C., Maire, E., Schöberl, E., Otero, F., Mesquita, F., Sinclair, I., et al., "Detailed Experimental Validation and Benchmarking of Six Models for Longitudinal Tensile Failure of Unidirectional Composites," *Composite Structures*, Vol. 279, Jan. 2022, Paper 114828. https://doi.org/10.1016/j.compstruct.2021.114828

[11] Wisnom, M., "Size Effects in the Testing of Fibre-Composite Materials," *Composites Science and Technology*, Vol. 59, No. 13, 1999, pp. 1937–1957. https://doi.org/10.1016/S0266-3538(99)00053-6

[12] Ubamanyu, K., Ghedalia, D., Hasanyan, A. D., and Pellegrino, S., "Experimental Study of Time-Dependent Failure of High Strain Composites," *AIAA Scitech 2020 Forum*, AIAA Paper 2020-0207, 2020. https://doi.org/10.2514/6.2020-0207

[13] Long, Y., Rique, O., Fernandez, J. M., Bergan, A. C., Salazar, J. E., and Yu, W., "Simulation of the Column Bending Test Using an Anisotropic Viscoelastic Shell Model," *Composite Structures*, Vol. 288, May 2022, Paper 115376. https://doi.org/10.1016/j.compstruct.2022.115376

[14] Rodriguez, P. A., Murphey, T. W., Radford, D. W., and Kwok, K., "Predictive Engineering Tools for Modeling the Viscoelastic Response of High Strain Composites," *AIAA Scitech 2022 Forum*, AIAA Paper 2020-0650, 2022. https://doi.org/10.2514/6.2022-0650

[15] Yee, J., and Pellegrino, S., "Folding of Woven Composite Structures," *Composites Part A: Applied Science and Manufacturing*, Vol. 36, No. 2, 2005, pp. 273–278. https://doi.org/10.1016/s1359-835x(04)00167-8

[16] Yee, J., and Pellegrino, S., "Biaxial Bending Failure Locus for Woven-Thin-Ply Carbon Fibre Reinforced Plastic Structures," *46th AIAA/ASME/ASCE/AHS/ASC Structures, Structural Dynamics and Materials Conference*, AIAA Paper 2005-1811, 2005. https://doi.org/10.2514/6.2005-1811

[17] Sanford, G., Biskner, A., and Murphey, T., "Large Strain Behavior of Thin Unidirectional Composite Flexures," *51st AIAA/ASME/ASCE/AHS/ASC Structures, Structural Dynamics, and Materials Conference 18th AIAA/ASME/AHS Adaptive Structures Conference 12th*, AIAA Paper 2010-2698, 2010. https://doi.org/10.2514/6.2010-2698

[18] Sanford, G. E., Ardelean, E. V., Murphey, T. W., and Grigoriev, M. M., "High Strain Test Method for Thin Composite Laminates," *16th International Conference on Composite Structures*, FEUP, Porto, Portugal, 2011.

[19] Murphey, T., Sanford, G., and Grigoriev, M., "Nonlinear Elastic Constitutive Modeling of Large Strains in Carbon Fiber Composite Flexures," *16th International Conference on Composite Structures*, FEUP, Porto, Portugal, 2011.

[20] López Jiménez, F., and Pellegrino, S., "Folding of Fiber Composites with a Hyperelastic Matrix," *International Journal of Solids and Structures*, Vol. 49, Nos. 3–4, 2012, pp. 395–407. https://doi.org/10.1016/j.ijsolstr.2011.09.010

[21] Murphey, T. W., Peterson, M. E., and Grigoriev, M. M., "Large Strain Four-Point Bending of Thin Unidirectional Composites," *Journal of Spacecraft and Rockets*, Vol. 52, No. 3, 2015, pp. 882–895. https://doi.org/10.2514/1.a32841

[22] Medina, K., Rose, T., and Murphey, T. W., "Initial Investigation of Time Dependency on Failure Curvatures of FlexLam High Strain Composites," *Proceedings of the American Society for Composites—Thirty-Second Technical Conference*, DEStech Publ., Lancaster, PA, 2017. https://doi.org/10.12783/asc2017/15231

[23] Herrmann, K. M., "An Investigation of a Vertical Test Method for Large Deformation Bending of High Strain Composite Laminates," Master's Thesis, Dept. of Aeronautical and Astronautical Engineering, Univ. of Washington, Seattle, WA, 2017.

[24] Rose, T., Sharma, A., Seamone, A., López Jiménez, F., and Murphey, T., "Carbon Unidirectional Composite Flexure Strength Dependence on Laminate Thickness," *Proceedings of the American Society for Composites—Thirty-Third Technical Conference*, DEStech Publ., Lancaster, PA, 2018. https://doi.org/10.12783/asc33/26023

[25] Medina, K., Rose, T., and Francis, W., "Long-Term Stress Rupture Limitations of Unidirectionasl High Strain Composites in Bending," *Proceedings of the American Society for Composites–Thirty-Third Technical Conference*, DEStech Publ. Inc., Lancaster, PA, 2018. https://doi.org/10.12783/asc33/25922

[26] Fernandez, J. M., and Murphey, T. W., "A Simple Test Method for Large Deformation Bending of Thin High Strain Composite Flexures," AIAA Paper 2018-0942, 2018. https://doi.org/10.2514/6.2018-0942

[27] Rose, T., Medina, K., Francis, W., Kawai, K., and Fernandez, J., "Viscoelastic Behaviors of High Strain Composites," *2019 AIAA Spacecraft Structures Conference*, AIAA Paper 2019-2027, 2019. https://doi.org/10.2514/6.2019-2027

[28] Sharma, A. H., Rose, T., Seamone, A., Murphey, T. W., and López Jiménez, F., "Analysis of the Column Bending Test for Large Curvature Bending of High Strain Composites," *AIAA Scitech 2019 Forum*, AIAA Paper 2019-1746, 2019. https://doi.org/10.2514/6.2019-1746

[29] Firth, J. A., and Pankow, M. R., "Minimal Unpowered Strain-Energy Deployment Mechanism for Rollable Spacecraft Booms: Ground Test," *Journal of Spacecraft and Rockets*, Vol. 57, No. 2, 2020, pp. 346–353. https://doi.org/10.2514/1.a34565

[30] Schlothauer, A., Pappas, G. A., and Ermanni, P., "Material Response and Failure of Highly Deformable Carbon Fiber Composite Shells," *Composites Science and Technology*, Vol. 199, Oct. 2020, Paper 108378. https://doi.org/10.1016/j.compscitech.2020.108378

[31] Adamcik, B., Firth, J., Pankow, M., and Fernandez, J. M., "Impact of Storage Time and Operational Temperature on Deployable Composite Booms," *AIAA Scitech 2020 Forum*, AIAA Paper 2020-1183, 2020. https://doi.org/10.2514/6.2020-1183

[32] Kang, J. H., Hinkley, J. A., Gordon, K. L., Thibeault, S. A., Bryant, R. G., Fernandez, J. M., Wilkie, W. K., Morales, H. E. D., Mcgruder, D. E., Peterson, R. S., et al., "Viscoelastic Characterization of Polymers for Deployable Composite Booms," *Advances in Space Research*, Vol. 67, No. 9, 2020, pp. 2727–2735. https://doi.org/10.1016/j.asr.2020.07.039

[33] Gomez-Delrio, A., "Viscoelastic Analysis of High Strain Composites for Deployable Structures in Space Applications," M.Sc. Thesis, Univ. of Central Florida, Orlando, FL, 2020.

[34] Zehnder, A., Patel, V., and Rose, T., "Micro-CT Imaging of Fibers in Composite Laminates under High Strain Bending," *Experimental Techniques*, Vol. 44, No. 5, 2020, pp. 531–540. https://doi.org/10.1007/s40799-020-00374-9

[35] Sharma, A. H., Perez, R., Bearns, N. W., Rose, T., and López Jiménez, F., "Some Considerations Involving Testing Guidelines for Large Curvature Bending of High Strain Composites Using the Column Bending Test," *AIAA Scitech 2021 Forum*, AIAA Paper 2021-0196, 2021. https://doi.org/10.2514/6.2021-0196

[36] Ubamanyu, K., and Pellegrino, S., "Nonlinear Behavior of IM7 Carbon Fibers in Compression Leads to Bending Nonlinearity of High-Strain Composites," *AIAA Scitech 2023 Forum*, AIAA Paper 2023-0580, 2023. https://doi.org/10.2514/6.2023-0364

[37] Hasanyan, A. D., and Pellegrino, S., "Modeling of Damage in Coilable Composite Shell Structures," *AIAA Scitech 2023 Forum*, AIAA Paper 2023-0364, 2023.

[38] Aller, B., Pellegrino, S., Kinkaid, N., Mejia-Ariza, J., Otis, R., Chan, P., and Pena, F., "Strain Measurement in Coilable Thin Composite Shells with Embedded Fiber Bragg Grating Sensors," *AIAA Scitech 2023 Forum*, AIAA Paper 2023-2399, 2023. https://doi.org/10.2514/6.2023-2399

[39] Royer, F., and Pellegrino, S., "Experimentally Probing the Stability of Thin-Shell Structures Under Pure Bending," *Philosophical Transactions of the Royal Society A*, Vol. 381, No. 2244, 2023, Paper 2022-0024. https://doi.org/10.1098/rsta.2022.0024

[40] Yu, T., and Hanna, J., "Exact and Approximate Mechanisms for Pure Bending of Sheets," *Mechanism and Machine Theory*, Vol. 149, July 2020, Paper 103805. https://doi.org/10.1016/j.mechmachtheory.2020.103805.

[41] Gao, J., Chen, W., Chen, J., Hu, J., Zhao, B., Zhang, D., Fang, G., and Peng, F., "Accuracy Analysis on Counterweight-Balanced Column Bending Test," *Experimental Mechanics*, Vol. 62, Jan. 2022, pp. 137–150. https://doi.org/10.1007/s11340-021-00767-w

[42] Curtis, G., Milne, J., and Reynolds, W., "Non-Hookean Behaviour of Strong Carbon Fibres," *Nature*, Vol. 220, No. 5171, 1968, pp. 1024–1025. https://doi.org/10.1038/2201024a0

[43] Ishikawa, T., Matsushima, M., and Hayashi, Y., "Hardening Non-Linear Behaviour in Longitudinal Tension of Unidirectional Carbon Composites," *Journal of Materials Science*, Vol. 20, No. 11, 1985, pp. 4075–4083. https://doi.org/10.1016/0010-4361(86)90326-5

[44] Jones, W., and Johnson, J., "Intrinsic Strength and Non-Hookean Behaviour of Carbon Fibres," *Carbon*, Vol. 9, No. 5, 1971, pp. 645–655. https://doi.org/10.1016/0008-6223(71)90087-x

[45] Northolt, M., Veldhuizen, L., and Jansen, H., "Tensile Deformation of Carbon Fibers and the Relationship with the Modulus for Shear Between the Basal Planes," *Carbon*, Vol. 29, No. 8, 1991, pp. 1267–1279. https://doi.org/10.1016/0008-6223(91)90046-l

[46] Shioya, M., Hayakawa, E., and Takaku, A., "Non-Hookean Stress-Strain Response and Changes in Crystallite Orientation of Carbon Fibres," *Journal of Materials Science*, Vol. 31, No. 17, 1996, pp. 4521–4532. https://doi.org/10.1007/bf00366347

[47] Ueda, M., Saito, W., Imahori, R., Kanazawa, D., and Jeong, T.-K., "Longitudinal Direct Compression Test of a Single Carbon Fiber in a Scanning Electron Microscope," *Composites Part A: Applied Science and Manufacturing*, Vol. 67, Dec. 2014, pp. 96–101. https://doi.org/10.1016/j.compositesa.2014.08.021

[48] Van Dreumel, W. H., and Kamp, J. L., "Non Hookean Behaviour in the Fibre Direction of Carbon-Fibre Composites and the Influence of Fibre Waviness on the Tensile Properties," *Journal of Composite Materials*, Vol. 11, No. 4, 1977, pp. 461–469. https://doi.org/10.1177/002199837701100408

[49] Ueda, M., and Akiyama, M., "Compression Test of a Single Carbon Fiber in a Scanning Electron Microscope and its Evaluation via Finite Element Analysis," *Advanced Composite Materials*, Vol. 28, No. 1, 2019, pp. 57–71. https://doi.org/10.1080/09243046.2018.1433506

[50] Lopez Jimenez, F., "Numerical Modeling of Stress Concentration Around Failed Fibers in Unidirectional Composites," *AIAA Scitech 2021 Forum*, AIAA Paper 2021-0087, 2021. https://doi.org/10.2514/6.2021-0087

[51] Parıs, F., Correa, E., and Cañas, J., "Micromechanical View of Failure of the Matrix in Fibrous Composite Materials," *Composites Science and Technology*, Vol. 63, No. 7, 2003, pp. 1041–1052. https://doi.org/10.1016/S0266-3538(03)00017-4

[52] Ghayoor, H., Hoa, S. V., and Marsden, C. C., "A Micromechanical Study of Stress Concentrations in Composites," *Composites Part B: Engineering*, Vol. 132, Jan. 2018, pp. 115–124. https://doi.org/10.1016/j.compositesb.2017.09.009

C. Bisagni
Associate Editor